

Tracking Control of a Piezoceramic Actuator Using Neural Networks

Ying-Shieh Kung and Fu-Kai Tu
Department of Electrical Engineering
Southern Taiwan University of Technology
Tel: (06) 2533131 ext. 231 Fax:(06)2537461
E-mail: kung@mail.stut.edu.tw

Abstract

This paper is to study the tracking control of a piezoceramic actuator (PA). Due to the inherent hysteresis nonlinearity, the PA always causes position error in the open-loop system and instability in the closed-loop system. To remedy this problem, a new control method combining the feedforward and feedback controllers is proposed to improve the dynamic performance of the PA. In the feedforward controller design, the hysteresis nonlinearity of the PA is modeled by using Preisach model first. A database of input/output history and a neural networks architecture treated as the inverse function of Preisach model are also utilized in the feedforward controller. In the feedback controller design, a PI controller is used to regulate the error between the command input and system output. In experiment, the command of square wave, sinusoid wave or triangular wave is taken as the tested signal to validate the excellent performances of the proposed controller.

Keyword: Piezoceramic actuator, Neural networks, Tracking control, Preisach model.

1. Introduction

Piezoceramic actuators, in Fig. 1, with many advantages such as high stiffness, fast-frequency response and nanometer resolution [1] have been used in many applications that require precise positioning control in recent years. Application examples include scanning tunneling microscope [2], stepper, diamond turning machine, positioning lenses and mirrors in optical systems [3], and etc. However, piezoceramic materials also have the following drawbacks [1] of the mechanical properties, such as, non-linearity, hysteresis, creep and thermal variations. These drawbacks, especially the effect of hysteresis, often cause the positioning error and diminish the performance quality of machine equipment in the open-loop system. For example, the scanning tunneling microscope needs the compensations of both nonlinearity and hysteresis in the scanning process. In order to solve these problems, there have been amounts of research efforts in the past. Newcomb and Flinn [4] proposed a linear control technique by use of the charge instead of voltage as control input.

Although its hysteresis effect and linear relationship are apparently improved, it decreases the frequency of response. Jung and Kim [5] presented a feedforward control method to improve the scanning accuracy of a scanning tunneling microscope. However, it could not completely express the dynamic behavior of the PA because its hysteresis nonlinearity only considers the symmetry and local memory. In order to improve the dynamic performance of the PA, a new control method including the feedforward and feedback controllers is designed. The feedforward controller contains a database of input/output history and the neural network architecture to replace the inverse function of Preisach model. The feedback PI controller is used to increase the positioning accuracy of the PA. By using the neural networks technique to model the inverse function of Preisach model, the hysteresis behavior is improved, the position control is more accuracy, and the command tracking becomes faster response in the experiments. Moreover, the robust characteristic of the neural networks [6] also increases the quality of the control system. The experimental results of dynamic responses are provided to validate the proposed control method.

2. Theoretical Analysis

2.1 Mathematical model for piezoceramic hysteresis

The classical Preisach model [7] used to model the nonlinear hysteresis behavior of the PA is described as

$$y(t) = \iint_{\alpha \geq \beta} \mu(\alpha, \beta) \gamma_{\alpha\beta}[u(t)] d\alpha d\beta \quad (1)$$

where $y(t)$ is the output response of the PA; $\mu(\alpha, \beta)$ is a weighing function of Preisach model; \mathbf{a} and \mathbf{b} correspond to “up” and “down” switching values of the inputs, respectively; and $\mathbf{g}_b[u(t)]$ is similar to a two-position relay and represents a hysteresis operator, whose value is determined by \mathbf{a} , \mathbf{b} and input $u(t)$. When the input $u(t)$ is larger than \mathbf{a} , $\mathbf{g}_b[u(t)]$ is switched to the “up” position, and when the input $u(t)$ is less than \mathbf{b} , $\mathbf{g}_b[u(t)]$ is switched to the “down” position.

The input value $u(t)$ of the PA could be divided into two conditions: the monotonically increasing and

decreasing conditions [8]. The former condition corresponds to the ascending branches of hysteresis loops in Fig. 2, where the input of the PA changes from $\beta_0 \rightarrow \alpha_1 \rightarrow \beta_1 \rightarrow \alpha_2 \rightarrow \beta_2 \rightarrow u(t)$. The output displacement $y(t)$ is the sum of double integral of the weighing function $m(a,b)$ on the trapezoidal regions of R^+ in Fig. 3. The $g_{ab}[u(t)]$ value is 1 in the region $R^+(t)$ and is 0 out of the region $R^+(t)$. Therefore, equation (1) can be simplified as

$$\begin{aligned} y(t) &= \iint_{R^+(t)} m(a,b) da db \\ &= (\iint_{R_1(t)} + \iint_{R_2(t)} + \iint_{R_3(t)}) m(a,b) da db \\ &\triangleq [X(a_1, b_0) - X(a_1, b_1)] + [X(a_2, b_1) - X(a_2, b_2)] \\ &\quad + X(u(t), b_2) \end{aligned} \quad (2)$$

or, in general

$$\begin{aligned} y(t) &= \sum_{k=1}^N [X(a_k, b_{k-1}) - X(a_k, b_k)] + X(u(t), b_N) \\ &\underline{D} y_H + y_C \end{aligned} \quad (3)$$

where

$$X(\alpha, \beta) = \iint_{R(\alpha, \beta)} \mu(\alpha, \beta) d\alpha d\beta \quad (4)$$

is defined as Preisach function representing the change in output $y(t)$ as the input $u(t)$ changes from a to b

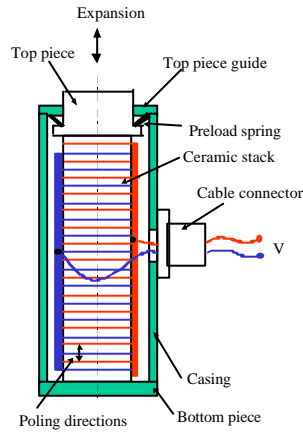


Fig.1 Piezoceramic Actuator

$y_H \triangleq \sum_{k=1}^N [X(a_k, b_{k-1}) - X(a_k, b_k)]$ is defined as the sum of output displacements for several switching input histories, and $y_C \triangleq X(u(t), b_N)$ is defined as the output displacement for current input on the ascending branch. Similarly, for the latter condition corresponds to the descending branches of hysteresis loops, if the input of the PA changes from $b_0 \rightarrow a_1 \rightarrow b_1 \rightarrow a_2 \rightarrow b_2 \rightarrow a_3 \rightarrow u(t)$, equation (1) can also be simplified as

$$\begin{aligned} y(t) &= \iint_{R^+(t)} m(a,b) da db \\ &= (\iint_{R_1(t)} + \iint_{R_2(t)} + \iint_{R_3(t)}) m(a,b) da db \\ &\triangleq [X(a_1, b_0) - X(a_1, b_1)] + [X(a_2, b_1) - X(a_2, b_2)] + [X(a_3, b_2) - X(a_3, u(t))] \end{aligned} \quad (5)$$

or, in general

$$\begin{aligned} y(t) &= \sum_{k=1}^{N-1} [X(a_k, b_{k-1}) - X(a_k, b_k)] + [X(a_N, b_{N-1}) \\ &\quad - X(a_N, u(t))] \underline{D} y_H + y_C \end{aligned} \quad (6)$$

where

$$y_H \underline{D} \sum_{k=1}^{N-1} [X(a_k, b_{k-1}) - X(a_k, b_k)] + X(a_N, b_{N-1})$$

and

$$y_C \underline{D} X(a_N, u(t)).$$

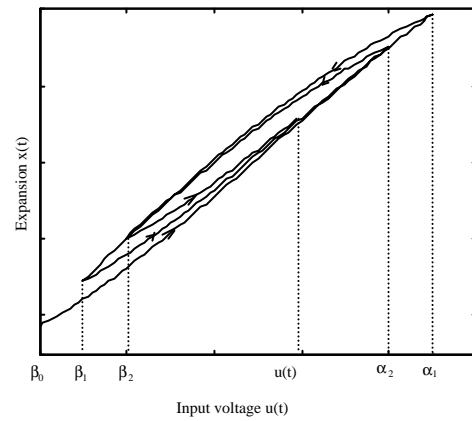


Fig. 2. The hysteresis loop of the PA with ascending branch.

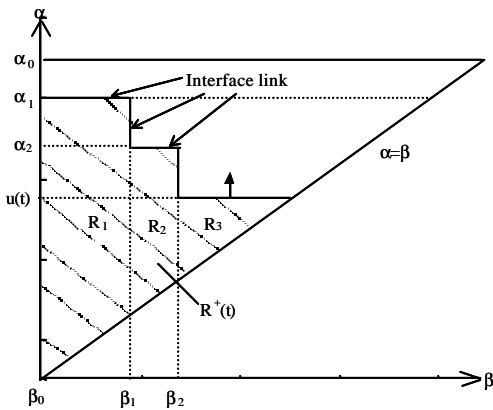


Fig. 3. The region $R^+(t)$ corresponds to the hysteresis loop shown in Fig. 2.

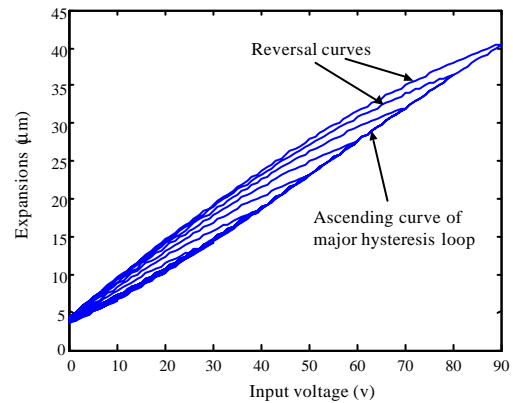


Fig. 4. The reversal curves of expansion displacements of the PA.

Equations (3) and (6), and the experimental data in Fig. 2 all show that the hysteresis behavior of the PA is 'non-local memory' because the current output displacement of the PA depends not only upon the current input but also upon the past several switching inputs. Basically, Preisach function $X(\alpha, \beta)$ in equations (3) and (6) can be obtained from the reversal curves of expansion displacements in experiments as shown in Fig. 4.

2.2 Controller design of the PA with the neural networks

To cope with the nonlinear hysteresis problem of the PA, a control algorithm combining the feedforward and feedback controllers is presented in Fig. 5. The new feedforward controller using the neural networks is designed to obtain the inverse function of Preisach model in equation (1) for the purpose that the multiplication of the transfer function of PA and the feedforward controller could approach 1. A feedback controller constructed by the PI controller is to compensate the error between the input command and output displacement of the PA. Referring to equations (3) and (6), the feedforward controller in Fig. 5 can be established according to the input being in the monotonically increasing or decreasing conditions.

(A) In the monotonically increasing condition:

From equation (3), let the output displacement of the PA be equal to the input command, $y = r$, and yield

$$X(u_f(t), \mathbf{b}_N) = r(t) - \sum_{k=1}^N [X(\mathbf{a}_k, \mathbf{b}_{k-1}) - X(\mathbf{a}_k, \mathbf{b}_k)] \quad (7)$$

$$\underline{D}r(t) - y_H$$

Therefore, the control effort of the feedforward controller is given as follows:

$$u_f(t) = X^{-1}(\beta_N, r(t) - y_H), \quad (8)$$

where $X^{-1}(\cdot)$ denotes the inverse Preisach function which is replaced by a three-layer feedforward neural networks. The inputs of $X^{-1}(\cdot)$ or the neural networks are \mathbf{b}_N and $r(t) - y_H$, the output is $u_f(t)$, and y_H is the sum of the output displacements for the past switching input history. Therefore, from equation (8), the parameters in Fig. 5 are $K_r = -1$, $h_N = \mathbf{b}_N$ and

$$y_H = \sum_{k=1}^N [X(\alpha_k, \beta_{k-1}) - X(\alpha_k, \beta_k)].$$

(B) In the monotonically decreasing condition:

From equation (6) and the same condition in the previous section, we have

$$X(\mathbf{a}_N, u_f(t)) = \sum_{k=1}^{N-1} [X(\mathbf{a}_k, \mathbf{b}_{k-1}) - X(\mathbf{a}_k, \mathbf{b}_k)] + X(\mathbf{a}_N, \mathbf{b}_{N-1}) - r(t) \underline{D}y_H - r(t) \quad (9)$$

The control effort of the feedforward controller is given as follows:

$$u_f(t) = X^{-1}(\alpha_N, y_H - r(t)). \quad (10)$$

All the symbols are denoted as the same as that in the increasing condition. The inputs of $X^{-1}(\cdot)$ or the

neural networks are α_N and $y_H - r(t)$, and the output is $u_f(t)$. Therefore, from equation (10), the parameters in Fig. 5 are $K_r = 1$, $h_N = \mathbf{a}_N$ and

$$y_H = \sum_{k=1}^{N-1} [X(\mathbf{a}_k, \mathbf{b}_{k-1}) - X(\mathbf{a}_k, \mathbf{b}_k)] + X(\mathbf{a}_N, \mathbf{b}_{N-1}).$$

The inverse Preisach function $X^{-1}(\alpha, \beta)$ in equations (8) and (10) is replaced by a three-layer feedforward neural networks. The procedure of the forward computation for the neural networks can refer to [6] and is omitted here. The net connection weights, W_{ji}^k , in the networks can be determined according to the following training procedure:

- ① Set the possible input voltage range during operation as:

$$u_{\min} \leq u \leq u_{\max}. \quad (11)$$

- ② Within the range of equation (11), u is divided into M sets with a fixed step size (corresponding to the value of α_i , $i=1, 2, \dots, M$),

and the voltage-displacement data pairs $[\alpha_i, y_i]$ can be collected from the ascending curves of major hysteresis loop in Fig. 4. In similarity, for each reversal curve, voltage-displacement data pairs $[\beta_j, y_j]$, $j=1, 2, \dots, m$, can also be collected.

Therefore, the output value of Preisach function from switching input voltage α_i to β_j in each reversal curve can be obtained by calculating $X(\alpha_i, \beta_j) = y_i - y_j$. For all reversal curves in Fig. 4, the total collected data can be rearranged by two data sets. One data set has the input vector $\mathbf{Q}_1 = [\mathbf{a}_i, X(\mathbf{a}_i, \mathbf{b}_j)]$ and the output vector $\mathbf{Y}_1 = \mathbf{b}_j$, and the other data set has the input vector $\mathbf{Q}_2 = [\mathbf{b}_i, X(\mathbf{a}_i, \mathbf{b}_j)]$ and the output vector $\mathbf{Y}_2 = \mathbf{a}_j$ with $i=1, 2, \dots, M$ and $j=1, 2, \dots, m$. The total number of data sets is $N=2 \sum_{i=1}^M m_i$, where m_i

is the number of collected data for each reversal curve. The relation between input and output vectors can be regarded as a mapping problem of $\mathbf{Y} = f(\mathbf{Q})$, $\mathbf{Q} \in \mathbb{R}^n$, $n=2$, $\mathbf{Y} \in \mathbb{R}^m$, $m=1$. Obviously, the exact mathematical expression for this map is difficult. Fortunately, it is usually possible to closely approximate this map via a neural net learning [6].

- ③ From the above known data pairs $\{(\mathbf{Q}_1^i, \mathbf{Y}_1^i), i=1, 2, \dots, N/2\}$ and $\{(\mathbf{Q}_2^i, \mathbf{Y}_2^i), i=1, 2, \dots, N/2\}$, the connection weights W_{ji}^k , $k=2, 3$, which denote the connection from the i th node at layer $k-1$ to the j th node at layer k , are found using the backpropagation learning algorithm [6]. Therefore, $\hat{\mathbf{Y}} = N(\mathbf{Q})$ provides a structure that closely approximates the map of $\mathbf{Y} = f(\mathbf{Q})$. During the training process, the node number of the hidden

layer is determined according to the SSR of the learning errors, which is defined as:

$$SSR = \frac{1}{N} \sum_{i=1}^N (Y^i - \hat{Y}^i)^2 \quad (12)$$

Once the connection weights W_{ji}^k of a three-layer feedforward neural network are obtained, the control effort can be derived on line through the feedforward computation of the neural networks as shown in Fig.5.

A PI controller in Fig.5 is adopted as a feedback controller for the purpose of compensating the system uncertainty, load disturbance or mapping error of the neural networks. The digital PI control algorithm is given by

$$u_b(z^{-1}) = K_p e(z^{-1}) + \frac{K_I}{1-z^{-1}} e(z^{-1}) \quad (13)$$

where z^{-1} is the back shift operator, and K_p , K_I are proportional and integral gains, respectively.

3. Experiments and Results

The block diagram of the proposed control system is shown in Fig. 5, which consists of a PA, a position sensor, a power amplifier, an 12-bit A/D-D/A converter interface card and a computer, which is used to develop the control algorithm. The PA model is P-841.30 made by Physik Instrumente [3], and has a nominal expansion of 0~45 μ m under an input voltage of 0~100V. A position sensor of strain gauge attached to the PA has a linear resolution of 0.1~0.2%. The power amplifier converts the control voltage 0~10V to the range 0~100V for the PA with nonlinearity less than 0.5%.

The experimental results of hysteresis phenomenon of the P-841.30 PA are shown in Fig. 2. For constructing the neural networks to replace the inverse Preisach function of the control mode in Fig. 5, the voltage-displacement data pairs are collected and stored in computer via the A/D-D/A interface card. In our experiments, the voltage-displacement data pairs

for 9 reversal curves (descending curves) of the ascending curves of major hysteresis loop in Fig. 4 are collected. These reversal curves correspond 9 values of α_i with 10V, 20V,..., 90V. For each reversal curve with α_i , some points from α_i to 0 corresponding to the value of β_j with fixed step size of 1V are collected.

For example, the 91 values of β_j with 90V, 89V,..., 1V, 0V for the largest reversal curve ($\alpha_i=90$ V), or 11 values of β_j with 10V, 9V,..., 0V for the smallest reversal curve ($\alpha_i=10$ V) are collected.

In the control mode, using the collected voltage-displacement data pairs, we arrange it in the form that the input vector is $\mathbf{Q}=[\mathbf{Q}_1, \mathbf{Q}_2]^T$, the output vector is $\mathbf{Y}=[\mathbf{Y}_1, \mathbf{Y}_2]^T$ with $\mathbf{Q}_1=[\alpha_i, X(\alpha_i, \beta_j)]$, $\mathbf{Q}_2=[\beta_j, X(\alpha_i, \beta_j)]$, $\mathbf{Y}_1=\beta_j$, $\mathbf{Y}_2=\alpha_j$, $i=1, 2, \dots, 9$, $j=1, 2, \dots, m_i$, and where $X(\mathbf{a}_i, \mathbf{b}_j) = y_i - y_j$. Therefore, the total number of data sets is $N=2 \sum_{i=1}^M m_i = 2 \cdot (91+81+\dots, 11) = 918$. In Fig. 5, these

data pairs are used to train the connection weights W_{ji}^k in the neural networks and to replace the inverse Preisach function $X^{-1}(\alpha_i, \beta_j)$ in equations (8) and (10). In the implementations, to validate the effectiveness of the proposed controller, an input command of 10 Hz square wave with amplitudes of 9 μ m and 36 μ m in Fig. 5 is used to test the performances of the output responses and the controller schemes of the PI feedback controller only (regular PI controller), the neural networks feedforward controller only (NN controller alone) and the neural networks feedforward controller plus PI feedback controller (NN+PI controller), respectively. The sampling frequency of the control loop is 2 kHz and the output responses in different controller schemes are shown in Figs. 6-7.

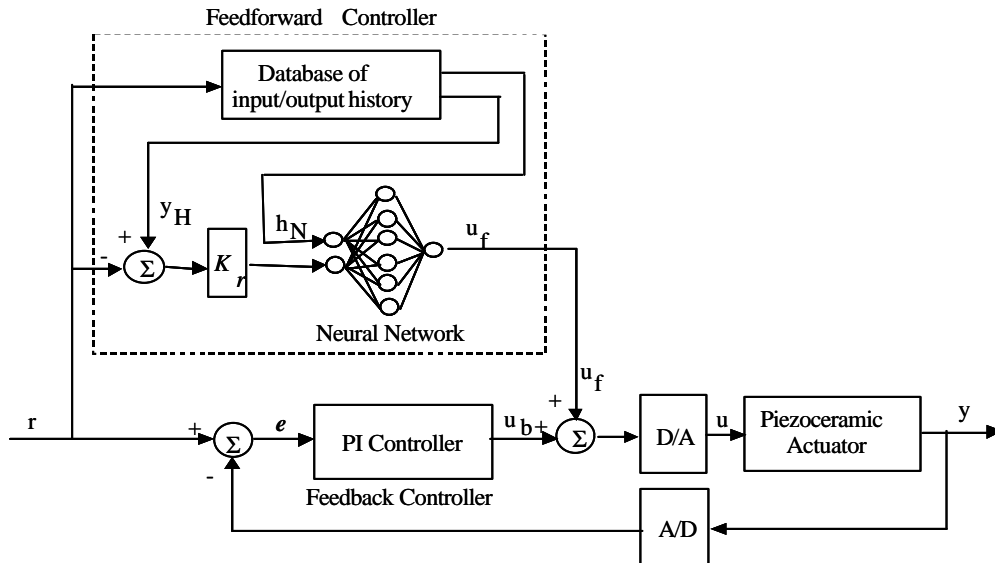


Fig. 5. The neural networks feedforward and PI feedback controllers.

Figure 6 shows that the effect of hysteresis phenomenon causes a large asymmetric steady-state error in the open-loop actuator system, but the proposed controller (NN+PI controller) has a good command tracking with 2 ms rising time, 2.5 ms settling time and zero steady-state error. Fig. 7 shows that in the case of the NN controller alone, it has a steady-state error with $0.45 \mu\text{m}$ at $36 \mu\text{m}$ position command input or $0.09 \mu\text{m}$ at $9 \mu\text{m}$ position command input. In the case of the regular PI controller, its response is slower than the other two controllers and has a little oscillation in transient state. Only the proposed NN+PI controller has the best characteristics with fast command regulation and zero steady-state error. To further compare the tracking control performance among the regular PI controller, the NN controller alone and the NN+PI controller, the input signals using the sinusoid wave with a amplitude of $27 \mu\text{m}$ (bias $22.5 \mu\text{m}$) and different signal frequencies for 20 and 100 Hz were employed. In Fig.5, the sampling frequency is 1.5 kHz in the input command and the neural-network feedforward control loop, but is 3 kHz in the PI feedback control loop. The tracking results

are plotted in Figs. 8~9. In the low-frequency tracking, such as a 20 Hz sine wave of the input command, three control schemes shown in Fig. 8 all have a good command tracking. The tracking error via the NN controller alone is the largest value, which are $1.76 \mu\text{m}$ peak-to-peak tracking error and $0.3203 \mu\text{m}^2$ error variance. The NN+PI controller with $0.91 \mu\text{m}$ peak-to-peak tracking error and $0.071 \mu\text{m}^2$ error variance has the best tracking performances. In a higher-frequency tracking, such as the 100 Hz sine wave of input command, Fig. 9 shows that the NN+PI controller possesses a low decay value and a smaller tracking error than that of the regular PI controller. It demonstrates that the proposed controller have a good tracking accuracy in high- frequency response.

To test the hysteresis ratio, the input signals using the triangular wave with a amplitude of $36 \mu\text{m}$ and a frequency of 10 Hz are employed. It is shown in Fig. 10 that the hysteresis ratio is decreased from a open-loop system with a maximum deviation 17% to a proposed closed-loop control system with a maximum one 0.8%.

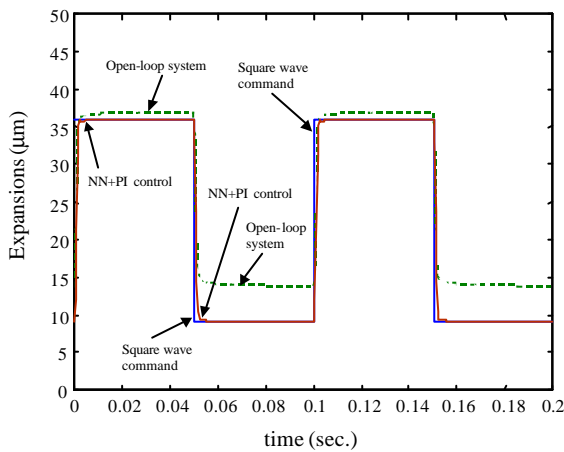


Fig. 6. Output responses of an open-loop system and the proposed NN+PI controller.

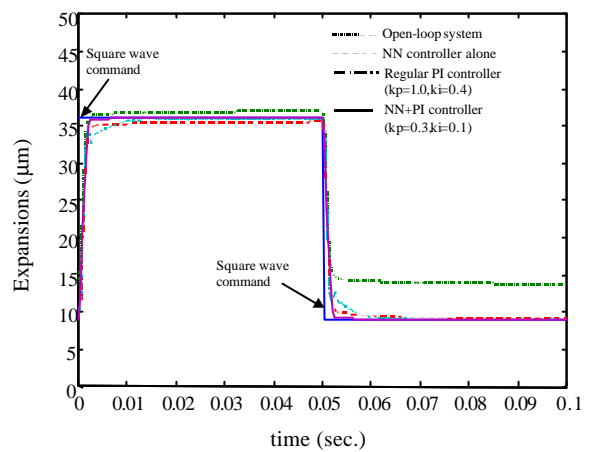


Fig. 7. Comparing the output responses of different control schemes

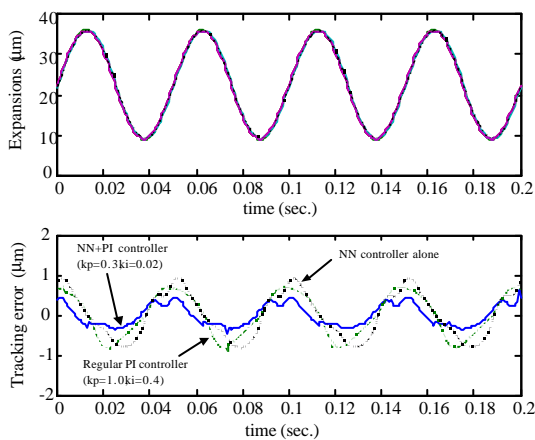


Fig. 8. The tracking results of different controllers with a 20Hz sinusoid input signal.

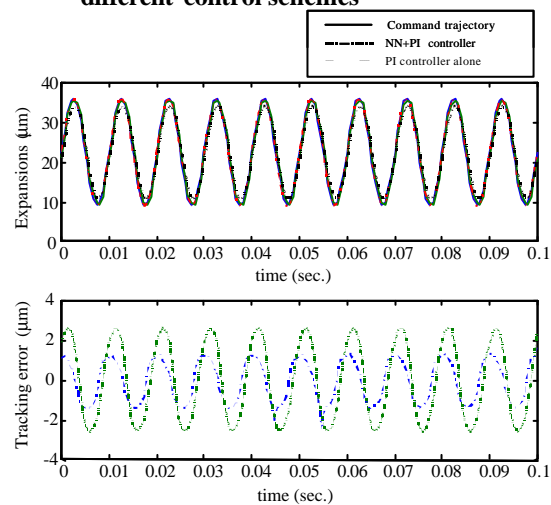
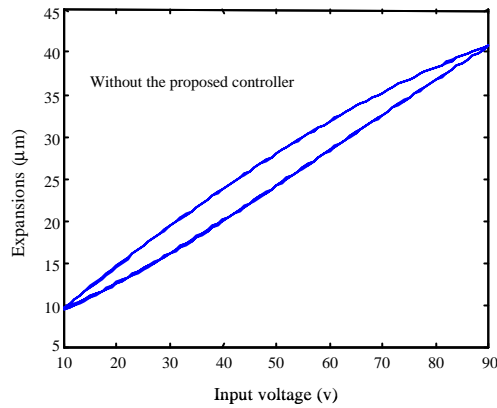
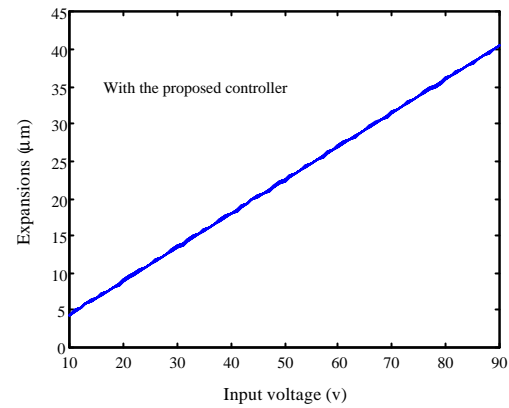


Fig. 9. Comparison of a regular PI controller and a NN+PI controller for tracking a 100Hz sinusoid input signal.



(a)



(b)

**Fig. 10. (a) The hysteresis phenomenon in the open-loop control.
(b) The linear result is improved by the proposed controller.**

4. Conclusions

A controller based on the neural network technique for the PA have been presented. In controller design, an architecture with both feedforward and feedback controllers is adopted. The feedforward controller is used for the inverse function of Preisach model and the feedback controller is used to regulate the errors between the input commands and output responses. From experimental results, the output expansions can track input commands perfectly, and the nonlinear hysteresis phenomenon can be improved well. The effectiveness of the proposed controller is then confirmed.

5. References

- [1] T. G. King, M. E. Preston, B. J. M. Murphy and D. S. Cannell, "Piezoelectric Ceramic Actuators: A Review of Machinery Applications," Precision Engineering, Vol. 12, No. 3, pp. 131-136, 1990.
- [2] D. Sarid, "Scanning Force Micoscopy-with Applications to Electric, Magnetic and Atomic Forces," New York Oxford, 1991.
- [3] Instrumete Physik, Products for Micro-positioning Catalogue, Edition E, 1995.
- [4] C. Newcomb and I. Flinn, "Improving the Linearity of Piezoelectric Ceramic Actuators," Electronics Letters, Vol. 18, No. 11, pp. 442-444, 1982.
- [5] S. Jung and S. Kim, "Improvement of Scanning Accuracy of PZT Piezoelectric Actuators by Feedforward Model-reference Control," Precision Engineering, Vol. 16, No. 1, pp. 49-55, 1994.
- [6] M. T. Hagan, H.B. Demuth, M. Beale, Neural Network Design, PWS Publish Company, 1996.
- [7] I. Mayergoyz, Mathematical Models of Hysteresis, New York: Springer-Verlag, 1991.
- [8] P. Ge and M. Jouaneh, "Modeling Hysteresis in Piezoceramic Actuators," Precision Engineering, Vol. 17, No.3, pp.211-221, 1995.

6. Acknowledgment

This work was supported by National Science Council under grant no. NSC-89-2213-E-218-019.

應用類神經網路在壓電陶瓷致動器之追蹤控制

龔應時、涂富凱
南台科技大學電機工程系

摘要

本文主要研究壓電陶瓷致動器之追蹤控制。由於壓電陶瓷致動器本身的磁滯非線性現象，以致於在開迴路控制時常造成定位之誤差或在閉迴路控制時常造成系統之不穩定狀況。為了解決此問題，本文提出一個結合前向及迴饋控制器之控制法則來改善壓電陶瓷致動器之動態性能。在前向控制器設計中，首先利用 Preisach 模式來構模壓電陶瓷致動器的磁滯非線性特性，接著，以一個輸出入歷史軌跡資料庫及類神經網路架構來建構 Preisach 模式之反函數。在迴饋控制器設計中，PI 控制器作為命令輸入及系統輸出間誤差的調節器。實驗中，方波、弦波及三角波命令之追蹤響應將作為驗證所提控制器的優越性。

關鍵詞： 壓電陶瓷致動器、類神經網路架構、追蹤控制、Preisach 模式。